



Differences in representation of extreme precipitation events in two high resolution models

Thomassen, Emma Dybro; Kendon, Elizabeth J.; Sørup, Hjalte Jomo Danielsen; Chan, Steven C.; Langen, Peter L.; Christensen, Ole B.; Arnbjerg-Nielsen, Karsten

Published in:
Climate Dynamics

Link to article, DOI:
[10.1007/s00382-021-05854-1](https://doi.org/10.1007/s00382-021-05854-1)

Publication date:
2021

Document Version
Peer reviewed version

[Link back to DTU Orbit](#)

Citation (APA):
Thomassen, E. D., Kendon, E. J., Sørup, H. J. D., Chan, S. C., Langen, P. L., Christensen, O. B., & Arnbjerg-Nielsen, K. (2021). Differences in representation of extreme precipitation events in two high resolution models. *Climate Dynamics*, 57, Article 3029–3043. <https://doi.org/10.1007/s00382-021-05854-1>

General rights

Copyright and moral rights for the publications made accessible in the public portal are retained by the authors and/or other copyright owners and it is a condition of accessing publications that users recognise and abide by the legal requirements associated with these rights.

- Users may download and print one copy of any publication from the public portal for the purpose of private study or research.
- You may not further distribute the material or use it for any profit-making activity or commercial gain
- You may freely distribute the URL identifying the publication in the public portal

If you believe that this document breaches copyright please contact us providing details, and we will remove access to the work immediately and investigate your claim.

1 Differences in Representation of Extreme Precipitation Events in Two High Resolution Models

2 **Author list:** Emma D. Thomassen^{1,2,5}, Elizabeth J. Kendon³, Hjalte J. D. Sørup¹, Steven C. Chan^{4,5}, Peter L.
3 Langen⁶, Ole B. Christensen², Karsten Arnbjerg-Nielsen¹.

4 ¹ Department of Environmental Engineering, Technical University of Denmark, Kgs. Lyngby Denmark

5 ² Danish Meteorological Institute, Copenhagen, Denmark

6 ³ Met Office Hadley Centre, Exeter, UK

7 ⁴ School of Engineering, Newcastle University, Newcastle-upon-Tyne, UK

8 ⁵ Visiting Scientist at Met Office Hadley Centre, UK

9 ⁶ iClimate, Department of Environmental Science, Aarhus University, Roskilde, Denmark

10 Key words: Climate Models, Extreme Precipitation, Tracking, Event Evolution, Event Life cycle, Model
11 Resolution

12 Abstract

13 High resolution regional climate models are needed to understand how climate change will impact extreme
14 precipitation. Current state-of-the-art climate models are Convection Permitting Models (CPMs) at kilometre
15 scale grid-spacing. CPMs are often used together with convective parameterised Regional Climate Models
16 (RCMs) due to high computational costs of CPMs. This study compares the representation of extreme
17 precipitation events between a 12km resolution RCM and a 2.2km resolution CPM. Precipitation events are
18 tracked in both models, and extreme events, identified by peak intensity, are analysed in a Northern European
19 case area. Extreme event tracks show large differences in both location and movement patterns between the
20 CPM and RCM. This indicates that different event types are sampled in the two models, with differences
21 extending to much larger scales. We visualise event-development using area-intensity evolution diagrams. This
22 reveals that for the 100 most extreme events, the RCM data is likely dominated by physically implausible
23 events, so called ‘grid-point storms’, with unrealistically high intensities. For the 1,000 and 10,000 most
24 extreme events, intensities are higher for CPM events, while areas are larger for RCM extreme events. Sampling
25 extreme events by season shows that differences between RCM and CPM in intensity and area in the top 100
26 extreme events are largest in autumn and winter, while for the top 1,000 and top 10,000 events differences are
27 largest in summer. Overall this study indicates that extreme precipitation projections from traditional coarse
28 resolution RCMs need to be used with caution, due to the possible influence of grid-point storms.

29 1. Introduction

30 Climate change is likely to impact the magnitude and frequency of extreme precipitation (IPCC 2012). With a
31 warmer climate, the atmosphere is able to hold more moisture, which is expected to increase the intensity of
32 extreme precipitation events (Trenberth et al. 2003). This is well aligned with findings from previous studies,
33 which have found an increase in the intensity of extreme precipitation events (Christensen and Christensen
34 2003; Kendon et al. 2014; Prein et al. 2017c). Less certain is it how climate change will impact the frequency
35 and duration of extreme precipitation events, as many factors are controlling these, including large-scale
36 circulation patterns (Trenberth et al. 2003). Information on future extreme precipitation is needed to adapt to
37 climate change, including building resilient cities and minimising flood risk, and to inform mitigation decisions
38 (Semadeni-Davies et al. 2008; Urich and Rauch 2014; Rosenzweig et al. 2019).

39 Climate models are the main tool to project and understand changes in future climate, including extreme
40 precipitation (Frei et al. 2006), with the scale at which changes occur being of great importance. Extreme
41 precipitation at small temporal and spatial scales can have major impacts on society and cause pluvial flooding
42 (Archer and Fowler 2015; Thorndahl et al. 2017). Due to the importance of short-duration rainfall extremes and
43 the scale on which the processes leading to extreme precipitation occur, very high resolution climate models are
44 needed to provide reliable future projections (Kendon et al. 2012; Ban et al. 2014; Chan et al. 2014b; Sunyer et
45 al. 2017).

46 Regional changes in extreme precipitation can be inferred from three types of climate models; high resolution
47 Global Circulation Models (GCMs) with grid-spacing ~50km or less, Regional Climate Models (RCMs) with a
48 grid-spacing of ~10-50 km, with examples down to 5km (Lucas-Picher et al. 2012), and Convection-Permitting

49 Models (CPMs) with a grid-spacing $<5\text{km}$. While CPMs are also regional climate models, in the sense that they
50 span a limited area domain, they also differ from traditional RCMs by resolving convection explicitly as
51 outlined below. Throughout this study we use the terminology RCM to describe coarser resolution regional
52 models and CPM to describe higher resolution convection-permitting models. Both RCMs and CPMs are
53 currently used together, as there is often limited availability of CPM datasets and high computational costs
54 associated with running CPMs (Rummukainen 2010; Prein et al. 2015). As convective precipitation has a spatial
55 scale smaller than the RCM grid scale, a convective parameterisation scheme is needed, which aims to represent
56 the average effects of convection on the model grid. In contrast, CPMs represent convection explicitly, often
57 using no convective parameterisation scheme, due to the very high resolution (e.g. Kendon et al. 2012). In
58 particular, deep convective parameterisation is typically not used in CPMs, whilst the use of shallow convection
59 parameterisation varies between studies (Kendon et al. 2017). Several studies have found that the CPMs perform
60 better than RCMs in terms of the diurnal cycle of rainfall and the intensity, frequency and duration of sub-daily
61 extreme precipitation (Kendon et al. 2012; Prein et al. 2013; Chan et al. 2014c, b; Ban et al. 2014). Extreme
62 precipitation simulated in some RCMs has also been shown to be impacted by grid-point storms, which are
63 physically implausible events that occur when the scale of convection approaches the model grid-scale and the
64 assumptions of the convective parameterisation break down (Chan et al. 2014b). RCMs with a grid-scale of
65 approximately 10km are within the so-called “grey-zone”, where the assumptions underlying the convective
66 parameterisation become invalid (Molinari and Dudek 1992). We note, however, RCMs using scale-aware
67 convective schemes designed to operate in the grey zone would not be expected to have grid-point storms
68 (Kendon et al. 2021).

69 A tracking algorithm can provide information on the characteristics and evolution of precipitation events, which
70 is extremely valuable in assessing the underlying processes for rainfall generation; yet few studies have applied
71 tracking algorithms to long continuous CPM simulations (Caine et al. 2013; Prein et al. 2017b, a; Purr et al.
72 2019; Li et al. 2020; Caillaud et al. 2021). Prein et al. (2017a) found an increase in both the intensity and size of
73 future mesoscale convective systems (MCS) over North America analysing a CPM, indicating a doubling in the
74 risk of flooding. While Caine et al. (2013), Prein et al. (2017b), Purr et al. (2019), Li et al. (2020) and Caillaud
75 et al. (2021) analysed how well precipitation events are simulated in CPMs compared to observations, none of
76 the studies compared results from the analysed CPMs with RCM simulations. Few studies to date have applied
77 tracking algorithms to both CPMs and RCMs to identify differences in extreme precipitation event
78 characteristics and evolution across model resolution (Crook et al. 2019).

79 In this study we explore and quantify the differences in extreme event characteristics between a CPM and an
80 RCM, from the UK Met Office, over a northern European region. We examine the difference in the tracked
81 extreme events (consecutive rainfall areas with intensities above 1mm/hr) between the CPM and RCM and
82 develop a new method to simplify area-intensity evolution in diagrams. This method enables us to represent the
83 typical event evolution across many events with different durations and allows comparison of the representation
84 of extreme events between models or different time periods. Due to the lack of high-resolution (temporal and
85 spatial) gridded precipitation observations, it is not possible to provide an observational reference for event
86 evolution and thus we focus on the differences between the models. In particular, E-OBS, ERA5, IMERG
87 satellite data and radar products were all considered, but not used due to them being of too coarse resolution, not
88 continuous and/or of low data quality over the study area.

89 **2. Methods**

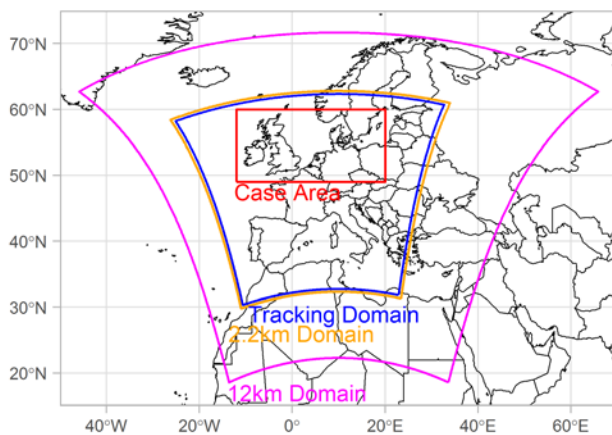
90 **2.1. Climate Model Data**

91 Two models are compared in their representation of extreme events, an RCM with a 12km horizontal resolution,
92 referred to as “RCM12” and a CPM with a 2.2km grid spacing, referred to as “CPM2”. The RCM12 and CPM2
93 are configurations of the Met Office Unified Model (UM), developed by the UK Met Office and are described
94 further in Berthou et al. (2018). Key differences between the two models are as follows:

- 95 - The RCM12 (UM version 10.3) is based on a climate version of the UM (Williams et al. 2018) and
96 uses a convection parameterisation based on Gregory and Rowntree (1990). The RCM12 has a model
97 time step of 4 minutes and uses a prognostic cloud fraction and condensate scheme (Wilson et al.
98 2008).

99 - The CPM2 (UM version 10.1) is based on the operational UKV Met Office model for numerical
100 weather predictions (Clark et al. 2016) and runs without any convection parameterisation (both shallow
101 and deep are switched off). The CPM2 has a model time step of 1 minute and uses the diagnostic
102 (Smith 1990) cloud scheme. The CPM2 includes prognostic graupel, which is a second category of ice
103 that has higher fall speeds and is typically found in convective clouds (unlike the RCM12 which just
104 has a single category of ice). The CPM2 uses a new blended boundary-layer parameterization (Boutle
105 et al. 2014a, b).

106 The RCM12 and CPM2 are in this analysis driven by the ERA-Interim reanalysis (Dee et al. 2011) and both
107 models directly downscale the driving model, hence the CPM2 model is not nested in the RCM12. Both model
108 simulations span a pan-European domain: the RCM12 and CPM2 model domains are shown in Fig. 1. For both
109 models, precipitation output is available at hourly resolution. 10 years of data from 1999-2008 is analysed. All
110 analyses are carried out with model output regridded to a common 12km grid (with mass conservation) for a
111 direct comparison of results. Furthermore, all analyses are performed also for model output regridded to a
112 common 25km grid, results from these analyses are found in Supplementary section 4.



113
114 **Fig. 1** Overview of data domain. Pink domain: 12km RCM12 data domain. Orange domain: 2.2 km CPM2 data domain.
115 Blue domain: Domain where tracking of events has been done. Red box: Case area for this study.

116 2.2. Tracking algorithm DYMECS

117 The DYMECS tracking algorithm was applied to output from both models at 12km resolution to identify
118 precipitation events and is described in detail in Stein et al. (2014). The algorithm was developed for UK radar
119 and Met Office convection-permitting forecast model precipitation data and has subsequently been applied to
120 climate model data by Crook et al. (2019). The algorithm was applied to rainfall fields within the common part
121 of the dataset (Tracking Domain, Fig. 1), removing 90 grid points (12km resolution) from each side of the
122 boundaries, still covering a large part of Europe. Events are defined as continuous rainfall fields above a certain
123 threshold and labelled based on “local table method” (Haralick and Shapiro 1992). Here an intensity threshold
124 of 1 mm/hour was used and with no areal threshold, allowing an event to be as small as one grid cell. Events are
125 tracked between two consecutive images (t and $t+1$) by displacing tracked elements in time t into time $t+1$ using
126 the velocity field $\mathcal{V}(t, t-1)$. The velocity field is based on windowed cross-correlations, dividing each image into
127 18×18 grid box windows (Rinehart and Garvey 1978). Analysing the overlapping areas between the advected
128 image of t and the image of $t+1$ tracks are identified using an overlap criterion of 0.6 (Stein et al. 2014). Settings
129 for the algorithm are similar to the settings Crook et al. (2019) used for precipitation tracking, though with a
130 slight adjustment of the size of the grid box window (18×18 instead of 20×20 , to fit the number of grid points in
131 the analysed domain).

132 The tracking algorithm considers birth, death, splitting and merging of events. Splitting describes the situation
133 where an event in time step t overlaps sufficiently with two events in time step $t+1$, hence the event splits into
134 two events. When two events at time step t both overlap sufficiently with one event in time step $t+1$, the events
135 are considered to have merged. In both splitting and merging, the event with the largest overlap keeps the
136 original event ID, while a new event ID is given in case of splitting (Crook et al. 2019). Splitting and merging of

137 events are kept track of by marking which event IDs are linked to a given event ID. In this study, an event is
138 defined by the period where it has the same ID in order not to account for the same part of an event twice.

139 The following event specific variables are extracted from the tracking algorithm and used to quantify extreme
140 precipitation from the two models:

- 141 - **Centroid Location [lat, lon, t]:** Centroid of fitted box around event area for each time step.
142 Parenthesis giving description and dimensions of variable.
- 143 - **Maximum Location [lat, lon, t]:** Location of the single maximum intensity cell for each time step.
- 144 - **Maximum Intensity [mm/hr, t]:** The maximum intensity of a single cell within the event for each
145 time step.
- 146 - **Mean Intensity [mm/hr, t]:** Average intensity over grid cells within the event (only grid cells with
147 intensities above 1 mm/hr are considered) for each time step.
- 148 - **Peak Maximum Intensity [mm/hr]:** Lifetime maximum intensity, based on the Maximum Intensity
149 variable for each event.
- 150 - **Peak Mean Intensity [mm/hr]:** Maximum mean intensity over the lifetime of each event, based on the
151 Mean Intensity variable.
- 152 - **Area [number of grid cells, t]:** Number of grid cells which are included in the event (only grid cells
153 with intensities above 1 mm/hr are considered) for each time step.
- 154 - **Maximum Area [number of grid cells]:** Lifetime maximum area for each event.
- 155 - **Box [lat min., lon min., n lat, n lon, t]:** A rectangular box fitted around all grid cells (> 1 mm/hr)
156 within the event at each time step [t]. The box is used only to identify the location of the event (used
157 for merging of events, section 2.5), but not used in the tracking. The size and location of the box fitted
158 around each event, is given by the bottom left corner [lat min, lon min] and size of the box [n lat, n
159 lon].

160 2.3. Extreme Event Definition

161 Extreme events are sampled from a Northern European case area in order to be able to compare seasonality and
162 movement of sampled extremes without mixing up different climatic zones. The Northern European case area is
163 defined between 12°W to 20°E and 49 to 60°N (see Fig. 1). An event is considered within the case area if its
164 Maximum Location is inside the case area at any time within the lifetime of the event. These events are all kept.
165 The entire lifetime of the event is then treated as an event within the case area despite the possibility that the
166 Maximum Location at some time steps is outside the case area. Extreme events which start and end at the
167 boundary of the tracking area are included, even though these may suffer from boundary artefacts impacting the
168 event evolution at the beginning or end of their lifetime. This is done to maintain the best possible extreme
169 distribution in the case area.

170 Extreme events are sampled from the population of events within the case area for further analysis. Here,
171 extreme events are defined based on their Peak Maximum Intensity (1-hour intensity) within the case area, and
172 the 10,000 most intense events are sampled in three bins, Top 100 (rank 1-100), Top 1,000 (rank 1-1,000), and
173 Top 10,000 (rank 1-10,000). Extreme events are furthermore sampled and analysed within each season.

174 2.4. Event Characteristics

175 Event characteristics are analysed for the Top 100 events in the RCM12 and CPM2 datasets considering four
176 variables: Area, Maximum Intensity, Mean Intensity and Volume. To study the evolution in event characteristics
177 for events with different lifetimes, the method proposed in Brisson et al. (2018) is used. Event lifetimes are
178 normalised to a range between 0 and 1 and the event characteristic for each time step in the event is extracted. A
179 second order polynomial is fitted to the event characteristic data for each of the Top 100 events. Brisson et al.
180 (2018) also suggested a normalisation of the variables, introducing the term var'_t :

$$181 \quad var'_t = \frac{var_t}{\overline{var}}$$

182 Where var is either Area, Maximum Intensity, Mean Intensity or Volume, var_t is the variable at the given time
183 step and \overline{var} is the mean value of the variable for the given event. Results with no normalisation of the variables

184 (only normalisation of lifetime) are presented in section 3.3, while results with normalisation of the variables are
185 presented in the Supplementary section 3.

186 **2.5. Merging of Events**

187 Merging of events is applied as a post processing step based on the results of the tracking algorithm. Events are
188 merged if the Box around two or more events are spatially overlapping or within a distance of 48km (4 grid
189 points) from each other at a single time step. Events are then merged for the entire lifetime of the events. The
190 merged event is given the event ID of the event with highest Peak Maximum Intensity, and information from
191 both events is merged. Area still only considers grid cells with intensities above 1mm/hr. Centroid Location is
192 calculated based on the new Box fitted around the merged event. The merging is done recursively (due to
193 updating of the Box around the merged event), until no further events are merged.

194 **2.6. Event Volume**

195 The total volume [m³] of rainfall associated with each event i , is defined as:

$$196 \text{ Event volume}_i = \sum_{t=1}^{\text{life}_i} \text{Mean Intensity}_{i,t} \cdot \text{Area}_{i,t}$$

197 The Event volume is calculated over the course of the entire event period, $t=1 \dots \text{life}_i$, defined as the period
198 where the event has the same ID, disregarding splitting and merging with events of other IDs. For events within
199 the case area the entire lifetime of the event is considered. The accumulated volume associated with events for a
200 given area is defined as:

$$201 \text{ Accumulated volume} = \sum_{i=1}^{\text{nTracks}} \text{Event volume}_i$$

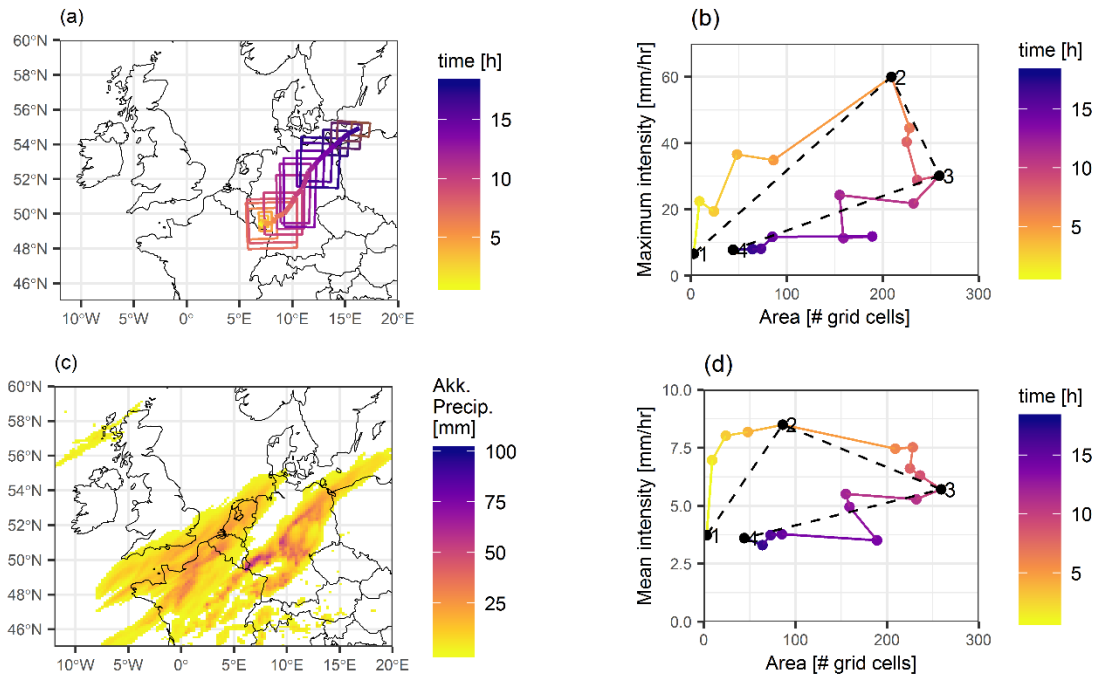
202 **2.7. Simplified Event Evolution (SEE)**

203 Area-intensity evolution diagrams have been used to describe the life cycle of the events, as seen in the case
204 from numerical weather predictions (Keat et al. 2019). In this study, we suggest a method to simplify the
205 evolution diagram across event durations, making it possible to create an average event evolution across
206 numerous events and therefore suitable in a climate context. Here the metric is used to describe event
207 representation in the two models. From the tracking algorithm the Area, Maximum Intensity and Mean Intensity
208 time series are used to visualise the evolution of an event (see Fig. 2 b,d). There are large variations in the event
209 evolution between events and for longer lifetimes the event evolution can be more complex (shown in
210 Supplementary section 1). In order to compare event evolutions across datasets, the evolution is simplified into
211 four points (see Fig. 2 b,d):

- 212 1. Birth: Size and intensity when the event is first detected.
- 213 2. Peak intensity: Size and intensity at the point where the event reaches its peak intensity.
- 214 3. Maximum area: Size and intensity when the event reaches its largest size (defined as the horizontal
215 area identified with the event [number of grid cells above threshold]).
- 216 4. Death: Size and intensity at the last time step the event is detected.

217 The simplified event evolution (SEE) is performed based on both Peak Maximum Intensity SEE_{max} (Fig. 2b) and
218 Peak Mean Intensity SEE_{mean} (Fig. 2d). Maximum Intensity is the maximum intensity of a single grid cell within
219 the event for each time step, whereas Mean Intensity is the mean intensity for all grid cells included in the event
220 for each time step.

221 The median SEE is calculated to compare the event evolution between different ranks of extreme events or
222 between models. First a simplified event evolution is fitted to each event in a sample of extreme events. Then a
223 median event evolution figure is created by finding the median of each of the four points (1. birth, 2. peak
224 intensity, 3. maximum area and 4. death) within the individual fitted simplified event evolution figures, both for
225 intensity (y-axis) and area (x-axis).



226
227
228
229
230
231

Fig. 2 Event evolution over time an event in the CPM2 dataset (2002-06-19 14:00 – 2002-06-20 07:00). a: Storm track with indication of area of the event over time. c: Accumulated rainfall over the event duration (footprint). b: Event evolution over time in maximum intensity and area (dots indicate hourly time steps and colour indicate time proceeding), with simplified event evolution based on maximum intensity in black. d: Event evolution over time for mean intensity and area (dots indicate hourly time steps and colour indicate time proceeding), with simplified evolution for mean intensity in black.

232 3. Results and Discussion

233 3.1. Sampled Extreme Events

234 A total of 4,219,064 events were tracked in the RCM12 dataset and 6,456,733 events were tracked in the CPM2
235 dataset for the entire tracking domain (see Fig. 1). Events which did not reach a larger area than 1 grid point
236 were removed, resulting in 2,494,326 RCM12 and 4,333,758 CPM2 events. Of these, 701,475 events (28%)
237 were located in the case area in the RCM12 dataset and 1,457,943 events (34%) in the CPM2 data (see Fig. 1,
238 red box). This corresponds to approximately 192 events per day in the RCM12 dataset and 399 events per day in
239 the CPM2 dataset. Due to the definition of events as consecutive rainfall areas, events in this study must be
240 considered distinctly different from large scale rainfall descriptions such as storms. The difference in number of
241 events between the two models is further discussed in Section 3.2.

242 Ranks were chosen to sample extreme events, in order to accommodate the different number of tracked events
243 between the two models. The 10,000 most intense events (based on the variable Peak Maximum Intensity) were
244 sampled in three categories, Top 100 (rank 1-100), Top 1,000 (rank 1-1,000), and Top 10,000 (rank 1-10,000).
245 Here an equal sample size is obtained between the two models, in the same way as sampling a specific number
246 of events per year. Based on the pool of events from each of the two models, the Top 100, Top 1,000 and Top
247 10,000 events correspond to percentiles ranging from 99.993-98.574 (Table 1). While the RCM12 dataset has
248 largest maximum intensity for Top 100, the CPM2 dataset show larger intensity for Top 1,000 and Top 10,000.

249

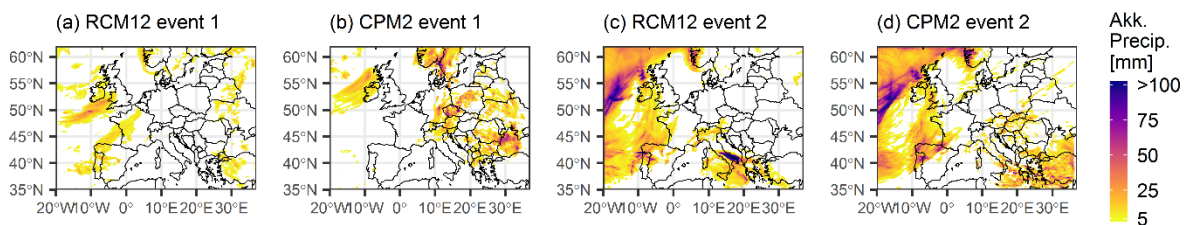
250 **Table 1** Percentile related to the sampled extreme events (>1mm/hr) and corresponding maximum intensities in mm/hr, after
 251 merging Top100 events. Maximum intensities represent the maximum intensity located inside the case area, lower ranked
 252 events can have higher intensities outside the case area.

	CPM2		RCM12	
	Percentile	Max intensity [mm/hr]	Percentile	Max intensity [mm/hr]
1 st	-	61.5	-	116.5
100 th	99.993	37.2	99.985	40.3
1,000 th	99.931	25.2	99.857	23.3
10,000 th	99.314	13.6	98.574	10.2

253

254 3.2. Merging of Events

255 Due to the different representation of rainfall in the two models, the number of events in the two models is not
 256 expected to be the same. Furthermore some of the expected difference between models can be explained purely
 257 by the difference in resolution. When comparing the same RCM12 and CPM2 simulations as studied here
 258 against observations, Berthou et al. (2018) found no clear signal of a better performance of one of the two
 259 models in terms of mean daily and hourly precipitation. Both models showed areas of better and worse
 260 performance compared to the other over the analysed areas of the UK, Germany and Spain. Results here,
 261 showing a very different number of events between the models (2,494,326 events in the RCM12 vs. 4,333,758
 262 events in the CPM2), suggest a difference in how the tracking algorithm is able to define and track events in the
 263 two models. We note that this difference is not reduced when regridding to a coarser grid at 25km resolution
 264 (Supplementary section 4). Analysing periods with high intensity rainfall between the two models shows that
 265 rainfall is more scattered in the CPM2 dataset (see examples in Fig. 3). As the event definition in the tracking
 266 algorithm is based on a continuous area of rainfall (>1mm/hr), this can lead to splitting events, which by eye
 267 could be classified as the same event. Here tracking is done using precipitation, while outgoing longwave
 268 radiation (OLR) is another well used method for tracking and detection of especially MCSs (e.g. Morel and
 269 Senesi 2002; Crook et al. 2019). OLR is smoother in space which would be likely to reduce the difference in the
 270 number of tracked events between the two models, but OLR tracking gives problems with false alarms as OLR
 271 is not a direct measurement of precipitation.



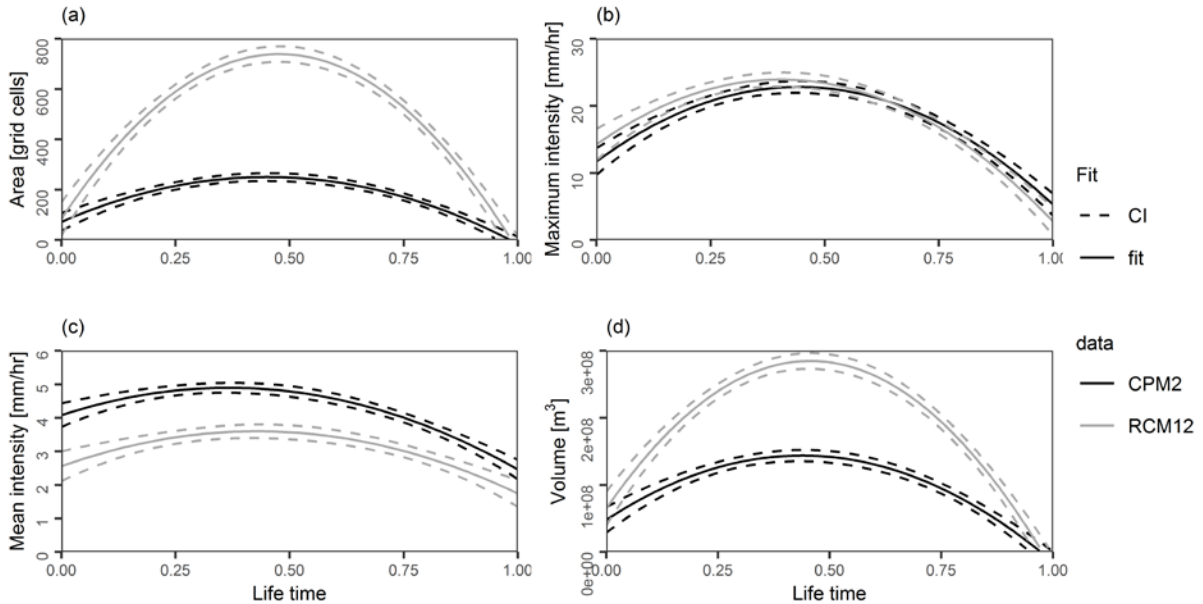
272 **Fig. 3** Footprint (accumulated rainfall) of periods with high intensity rainfall. (a) - (b) Event 1 from 18:30 10/08-2007 to
 273 18:30 11/08-2007 for RCM12 and CPM2 data respectively. (c) - (d) Event 2 from 05:30 19/09-2006 to 16:30 22/09-2006 for
 274 RCM12 and CPM2 data respectively.
 275

276 A scheme of merging events, as a post-processing step based on the tracking algorithm was tested on both
 277 model datasets. Events which at a certain time step were spatially very close to each other were merged with the
 278 aim of giving a better estimate of the number of independent events and reducing differences in the number of
 279 tracked events between the two models. However, the merging resulted in very large events and unrealistic
 280 event tracks due to rainfall often being spatially scattered over a large part of the domain. Therefore it was
 281 decided to only apply merging to events contributing to the sampled Top 100 set, in order to ensure that the 100
 282 most extreme events are not spatially overlapping or in close proximity and therefore cannot be considered the
 283 same event. The process of merging Top 100 events was done recursively until none of the selected 100 events
 284 could be further merged. A total of 14 Top 100 CPM2 events and 19 Top 100 RCM12 events were merged.
 285 After the merging the Top 100 CPM2 events consists of 89 independent days while the RCM12 Top 100 events

286 consists of 98 independent days¹. The merging of the Top 100 events ensures a more similar sample of events
 287 are compared between the two models. While sampling by rank is expected to give a fairer comparison of
 288 extreme events between the CPM2 and RCM12, some CPM2-RCM12 differences might be explained by the
 289 fewer events tracked in the RCM12. This will be discussed in the following sections along with the results.

290 3.3. Event Characteristics

291 Evaluating the characteristics of the Top 100 most intense events by Area, Maximum Intensity, Mean Intensity
 292 and Volume shows that the two models represent the Top 100 extreme events very differently. The RCM12 Top
 293 100 extreme events have higher peak values for Area and Volume compared to the CPM2 Top 100 events, while
 294 the opposite is the case for Mean Intensity (Fig. 4). No large differences are seen in the evolution of Maximum
 295 Intensity for the Top 100 most intense events between the two models. The largest difference between the
 296 RCM12 and CPM2 events is seen when comparing the Area and Volume of the Top 100 most intense extreme
 297 events. Although we note that, if variables were normalised, no differences between the models would be
 298 detected (see Supplementary Fig. 6). This suggest that the difference is scaled with the mean value e.g. the
 299 difference in the Area variable between the RCM12 and CPM2 is due to the difference in mean Area over the
 300 lifetime of the events. Differences between CPM2 and RCM12 Top 100 events in Mean Intensity are more
 301 modest, but show higher Mean Intensity for CPM2 Top 100 throughout the lifetime of the events (Fig. 4c). The
 302 larger areas for RCM12 events is somewhat expected, and could be explained by the convective scheme
 303 smoothing out precipitation leading to fewer individual events (Fig. 4a). More surprising is it that the CPM2
 304 events do not have higher Maximum Intensity compared to the RCM12 events, despite the convective scheme
 305 and higher original grid point resolution (Fig. 4b). The total Volume for the RCM12 Top 100 events are higher
 306 than for the CPM2 Top 100 events, which can be seen to mainly be influenced by the large difference in event
 307 area between the two models (Fig. 4d). Comparing these results to those where tracking has been applied to data
 308 regridded to 25km shows only small differences (Supplementary Fig. 8). In particular, model differences in the
 309 evolution of event characteristics are in general the same for the 25km data, although with smaller differences in
 310 Area and Volume, compared to those seen in Fig. 4 for the 12km data.



311 **Fig. 4** Evolution of Area (a), Maximum Intensity (b), Mean Intensity (c) and Volume (d) for Top 100 most intense events in
 312 the CPM2 dataset (black) and RCM12 dataset (grey). Event durations are normalised. The 99% Confidence Interval (CI) are
 313 shown with dashed lines.
 314

315
 316

¹ Unique days Top 1,000: 483 (CPM2), 582 (RCM12). Unique days Top 10,000: 1678 (CPM2), 2107 (RCM12).

317 **3.4. Volume**

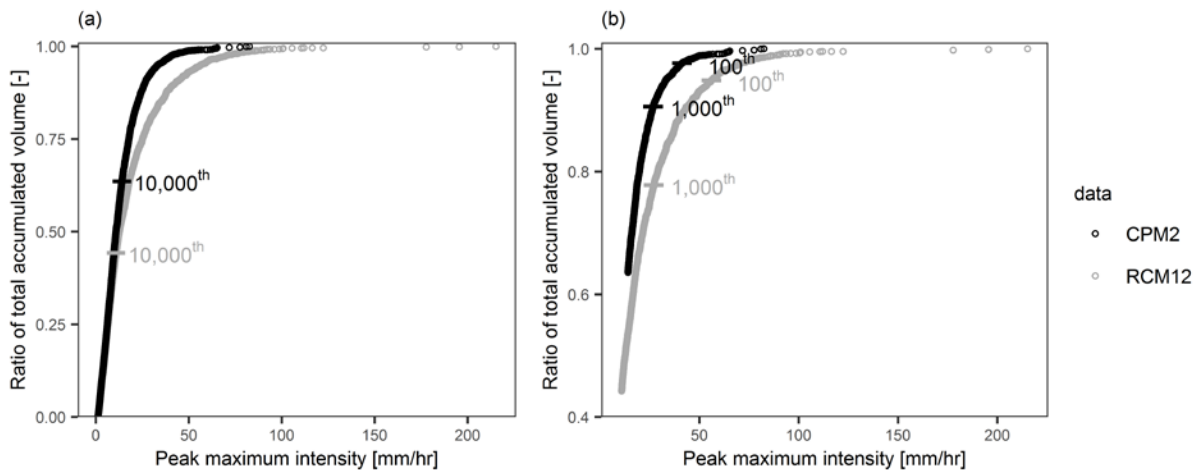
318 The Accumulated volume of all tracked events within the tracking domain (see Fig. 1) is approximately 11%
 319 higher in the CPM2 dataset than in the RCM12 dataset (Table 2). In contrast, for events within the Case area
 320 (Northern Europe – see Fig. 1) the total Accumulated volume is similar (only 2% larger in CPM2 dataset
 321 compared to the RCM12 dataset, Table 2). Considering only extreme events, the picture changes: the
 322 Accumulated volume for RCM12 extreme events is larger than for CPM2 extreme events, with increasing
 323 difference for more extreme events (Table 2). For Top 100 events, the Accumulated volume for the CPM2
 324 events is approximately 30% of the volume of RCM12 events (Table 2). The increasing difference in
 325 accumulated volume between the RCM12 and CPM2 for the most intense extreme events, suggests that this
 326 difference is not simply explained by the different number of tracked events between the two models. The same
 327 tendency is seen in the 25km data (Supplementary Table 2), although with smaller differences between RCM12
 328 and CPM2 events for the most severe extreme events.

329 **Table 2** Total volume accumulated for events in the CPM2 and RCM12 dataset (after removing single cell events).
 330 Definition of Tracking area and Case area are seen in Fig. 1. For all cases the entire lifetime of the event is considered in the
 331 total volume.

Accumulated Volume	CPM2 [10 ⁹ m ³]	RCM12 [10 ⁹ m ³]	Ratio [CPM2/RCM12]
Entire tracking area	52,483	47,183	1.11
Case area	22,332	21,894	1.02
Top 10,000	5,342	8,659	0.62
Top 1,000	1,013	2,616	0.39
Top 100	199	637	0.31

332

333 Considering all events in the case area, the contribution to the accumulated volume increases faster with
 334 maximum intensity in the CPM2 dataset compared to the RCM12 dataset (Fig. 5a), which is also seen for the 25
 335 km data (Supplementary Fig. 9). This shows that the most intense events sampled with the tracking algorithm
 336 contribute a smaller fraction of the total volume in the CPM2 dataset compared to the RCM12 dataset. As the
 337 CPM2 extreme events in general have smaller areas than the RCM12 events (Fig. 4a), this explains the lower
 338 total volume in the extreme events for the CPM2 compared to the RCM12 (Table 2). The 10,000 events with the
 339 highest maximum intensity represent a bit less than 40% of the total volume in the CPM2 dataset, while for the
 340 RCM12 dataset these events represents more than 55 % of the total volume in the dataset (Fig. 5b).



341 **Fig. 5** The contribution of events of increasing peak maximum intensity to the total accumulated volume (measured as the
 342 cumulative fraction) for all events (a) and for the 10,000 events with highest maximum intensity (b). Events are ranked by
 343 Peak Maximum Intensity. CPM2 dataset (black) and RCM12 dataset (grey). Marks indicate the rank 100, 1,000 and 10,000
 344 event for each of the datasets.
 345

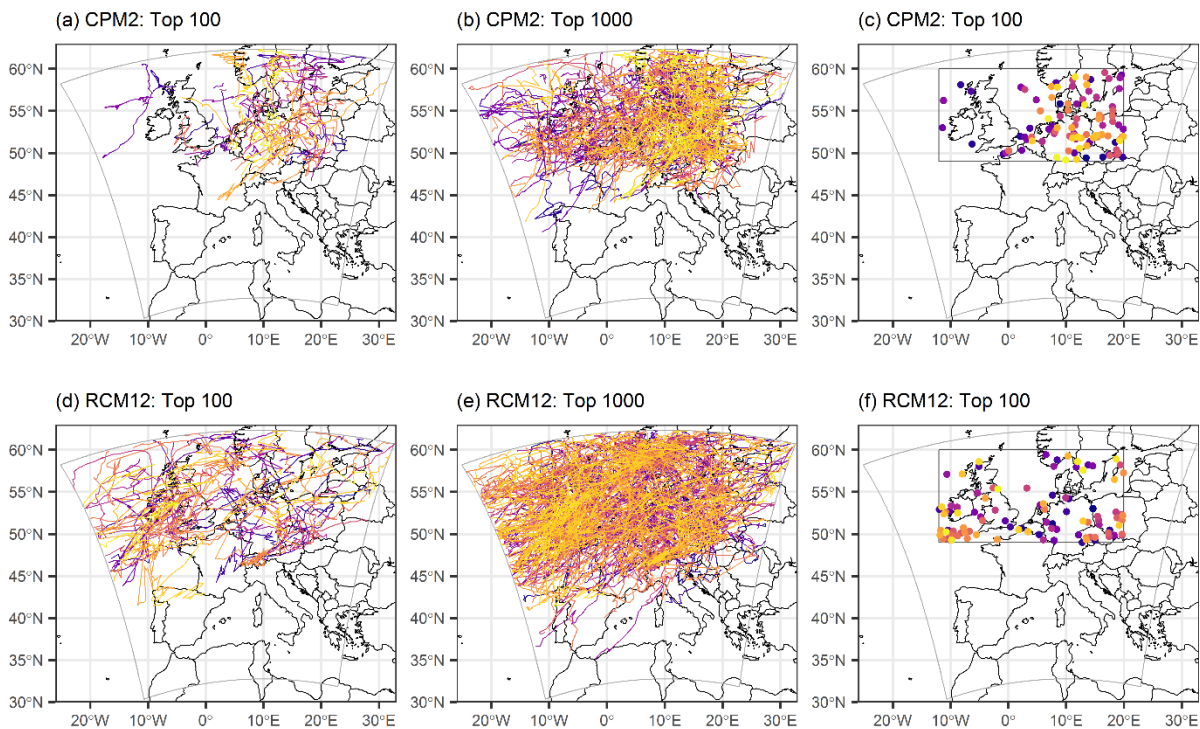
346

347

348 **3.5. Storm Tracks**

349 Tracks of the extreme events in the Northern European case area (Fig. 1, red box) are very different between the
 350 CPM2 and RCM12 (see Fig. 6). In the CPM2 dataset, the extreme events mostly occur over central Europe and
 351 southern Scandinavia (a-c) and tend to have a south to north (northward: 315-45°) direction of motion
 352 (Supplementary Fig. 4). By contrast, many of the extreme events in the RCM12 are located over the Atlantic
 353 Ocean and the British Isles (Fig. 6d-f) with a west to east (eastward) moving direction (Supplementary Fig. 4).
 354 Focussing on the maximum location inside the case area (Fig. 6c and f), CPM2 extreme events are mostly in the
 355 eastern part, whilst there is additionally a cluster of events in the western part in the RCM12. This indicates that
 356 some of the extreme events in the RCM12 are distinctly different from those in the CPM2. To understand these
 357 differences, the most intense extreme events in the CPM2 dataset are compared with tracks on the same day,
 358 with similar location and intensity, in the RCM12 dataset, and vice versa (see Supplementary section 2). From
 359 comparisons of tracks between the two models, we find:

- 360 - Extreme events from one dataset are rarely replicated by the other dataset, indicating completely
- 361 different sets of extreme events in the two models.
- 362 - Long event tracks in the RCM12 extreme set seem to be replicated well by the CPM2, though with
- 363 notably lower intensities, indicating that the RCM12 extreme set includes a group of events, which
- 364 according to the CPM2 are not extreme due to lower intensities.
- 365 - CPM2 extreme events are largely absent in the RCM12, with no tracks in the RCM12 with a similar
- 366 location and intensity on that day.



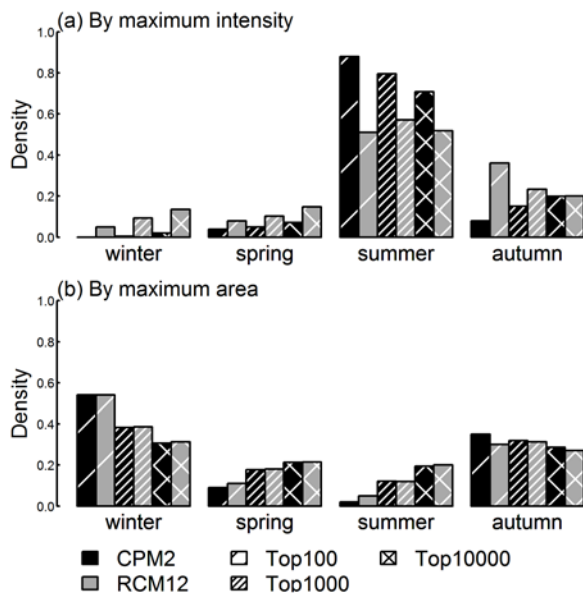
367 **Fig. 6** Storm tracks of Top 100 (rank 1-100, (a), (d)) and Top 1,000 (rank 1-1,000 (b), (e)) most severe events within the
 368 Northern European Case area. CPM2 dataset (a)-(c) and RCM12 dataset (d)-(f). (c), (f): Location of the Peak Maximum
 369 Intensity within the case area for the selected Top 100 most severe events. Colours distinguish different event tracks, plotted
 370 by rank in reverse order: least intense plotted first (dark colours), most intense plotted last (light colours). Note: Only events
 371 which have high intensities within the case area are shown.
 372

373 If events were instead sampled by their Peak Maximum Area (sampling of spatially large, but not necessarily
 374 intense events), there would be no visible difference in storm tracks between the two models (results shown in
 375 Supplementary section 3). The storm tracks of the spatially largest events have a large density of tracks over the
 376 British Isles and an eastward direction in both models. These tracks have very similar characteristics (both in
 377 terms of location and movement direction) as the tracks for events with the highest Peak Maximum intensity in
 378 the RCM12. Nevertheless, there is little overlap in events sampled by Peak Maximum intensity and Peak

379 Maximum Area in the RCM12 dataset (4, 13 and 23 % for Top 100, Top 1,000 and Top 10,000), though this
 380 overlap is larger than in the CPM2 dataset (0, 3 and 14 % for Top 100, Top 1,000 and Top 10,000). The better
 381 agreement in location between models for the spatially largest events compared to the most intense events, and
 382 the larger overlap between large and intense events in the RCM12 dataset, suggest that the group of extreme
 383 intense events in the RCM12 not seen as intense by the CPM2 are large events. Analysing the size of the events
 384 in the western cluster in the RCM12 data shows that the events in this cluster are on average double the size of
 385 the events in the eastern cluster. One plausible explanation for this group of extreme events in the RCM12 data,
 386 could be that the high intensities come from grid-point storms, occurring within large area events, which is a
 387 well-known problem in some RCMs (Chan et al. 2014a).

388 3.6. Seasonal Distribution

389 The seasonal distribution in the occurrence of extreme events shows a different pattern between the CPM2 and
 390 RCM12 dataset, again with largest differences for the most severe extreme events (Fig. 7a). The CPM2 dataset
 391 shows an increasing ratio of summer events on considering more extreme events (i.e. moving from Top10,000
 392 to Top100, significant with a chi-square homogeneity test, $p\text{-value} = 5.6 \cdot 10^{-12}$) which is not found in the
 393 RCM12 dataset. While the sample of CPM2 extreme events are highly dominated by summer events, RCM12
 394 extreme events have a higher ratio of events from other seasons. Sampling extreme events by Maximum Area
 395 shows no difference in the seasonal distribution in occurrence between the CPM2 and RCM12 (see Fig. 7b).
 396 This confirms that similar events are sampled in the two models when selecting by Maximum Area, whereas
 397 this is not the case when selecting by Maximum Intensity. Analysing characteristics of MCSs over Europe,
 398 Morel and Senesi (2002) found a larger density of MCSs over land than sea, with a clear concentration in the
 399 eastern part of the case area. This suggests that the representation of tracking location is closer to observations in
 400 the CPM2 dataset compared to the RCM12. MCSs in Northern Europe were found to have the highest frequency
 401 between May and August (Morel and Senesi 2002) which is in agreement with the seasonal distribution in both
 402 models, although more apparent in the CPM2. Morel and Senesi (2002) define MCSs as events reaching an area
 403 above 10,000km², while an areal threshold of 288km² (excluding single cell events) is used in this study with no
 404 attempt to distinguish between MCSs and non-MCSs. Yet Top 100 extreme events still reach an average area of
 405 750 grid cells (108,000km²) for RCM12 events and 200 grid cells (28,000km²) for CPM2 events (Fig. 4).

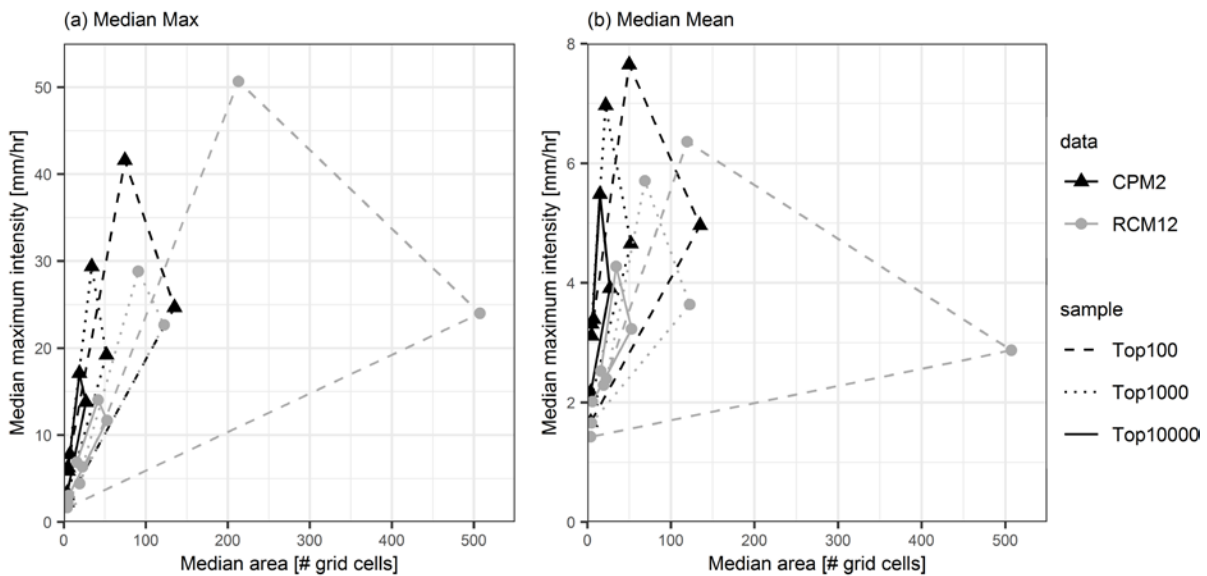


406
 407 **Fig. 7** Seasonal occurrence of maximum intensity events (a) and maximum area events (b). Events sampled in CPM2 dataset
 408 in black and events sampled in RCM12 dataset in grey.

409 3.7. Median Simplified Event Evolution

410 When comparing the median Simplified Event Evolution (SEE) of the extremes for the RCM12 and CPM2, it is
 411 clear that the event evolutions between the two models are very different (see Fig. 8). For Top 100 SEE_{max} the
 412 RCM12 extreme events reach higher intensities than the CPM2 events, while for Top 1,000 the median Peak
 413 Maximum Intensity is almost similar between the two models (Fig. 8a). When including more events (e.g. Top

414 10,000) the CPM2 extreme events reach higher median Peak Maximum Intensity than the RCM12 events (Fig.
 415 8a). This somewhat surprising higher Peak Maximum Intensity in the RCM12 dataset for the most severe
 416 extreme events is most likely caused by grid-point storms. These grid-point storms often occur within large
 417 scale areas of heavy precipitation, where the convective parameterisation breaks down, resulting in intensities
 418 above 100 mm/hr and a very low parameterized convective rainfall fraction for one or a few grid cells compared
 419 to surrounding grid cells. These grid-point storms are a known problem in some RCMs, which operate at grid
 420 scales smaller than those for which the convective parameterisation scheme was designed (see e.g. Chan et al.
 421 (2014b)). Both in size and intensity it is clear that the Top 100 extreme events in the RCM12 data have a very
 422 different event evolution than the Top 100 extreme events in the CPM2 data. These differences between models,
 423 both in terms of shape and values, become smaller for the median SEE_{max} for Top 1,000 and Top 10,000 events.
 424 While the area is still larger for the RCM12 events, the Maximum Intensity becomes higher for the CPM2
 425 events (Fig. 8a). For Top 1,000 and Top 10,000 SEE_{max} the difference in area between the two models could
 426 reasonably be described by the difference in how rainfall is modelled between the two models (convection being
 427 parameterised or not) and by the difference in the original resolution of the models. The Top 100 SEE_{max}
 428 confirms that a large part of the extreme events in the RCM12 dataset are very large events, and that these are
 429 not found in the CPM2 dataset. Together with findings from section 3.5 and section 3.6, we deduce that the
 430 RCM12 is overestimating the Maximum Intensity of these very large events due to the presence of grid-point
 431 storms (supported by an analysis of the convective fraction of rainfall above 100mm/hr in RCM12 events,
 432 Supplementary section 5). Regridding data to 25 km shows similar intensities between models for Top 100
 433 SEE_{max} while higher intensities for CPM2 Top 1,000 and Top 10,000. Areal differences follow the pattern seen
 434 in the 12km data with much larger arears for RCM12 Top 100 SEE_{max} compared to CPM2 Top 100 SEE_{max} .

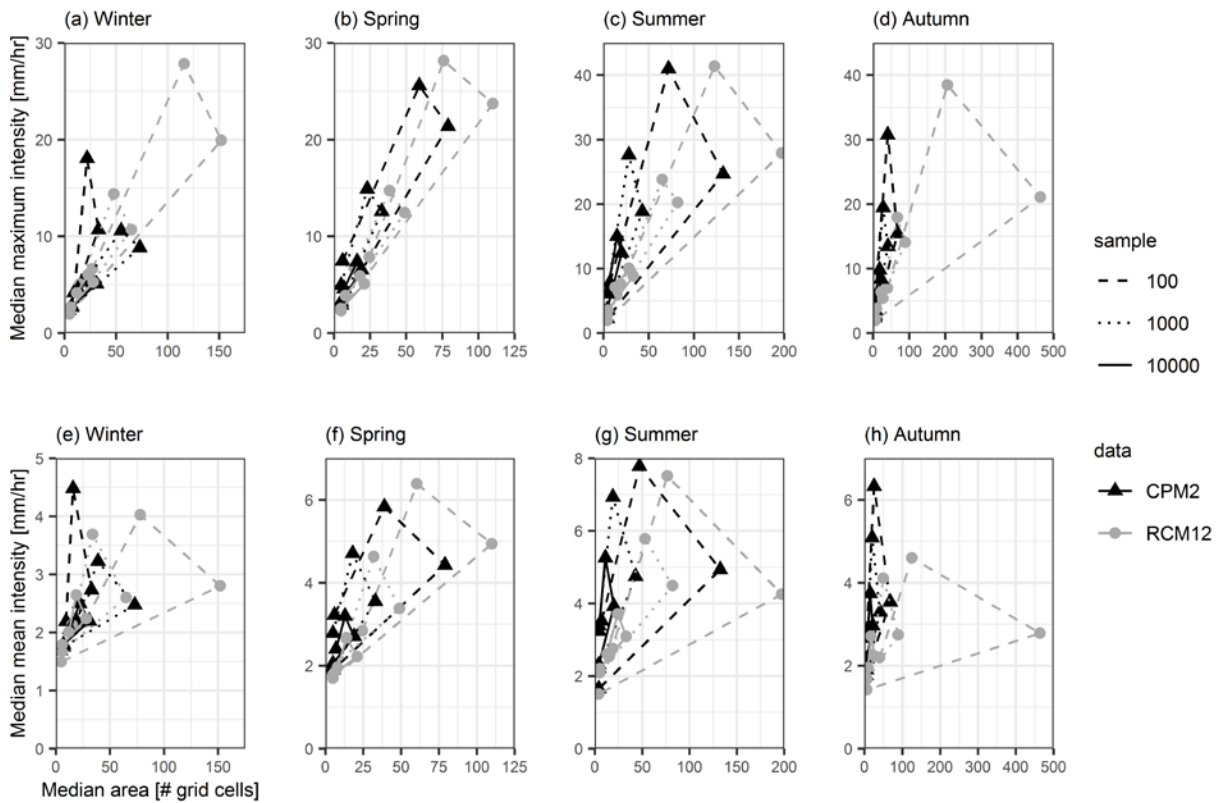


435
 436 **Fig. 8** Simplified median evolution based on maximum intensity (a) and mean intensity (b). Data for both CPM2 (black
 437 triangles) and RCM12 (grey circles). Severe events sampled based on maximum 1-hour intensity, Top 100 (dashed line),
 438 Top 1,000 (dotted line) and Top 10,000 (solid line).

439 For median SEE_{mean} the CPM2 extreme events have higher Mean Intensities than the RCM12 events, for all
 440 percentiles (Fig. 8b). As CPM2 extreme events are approximately half the size of corresponding RCM12
 441 extreme events, the CPM2 extreme events can be characterised as small and intense compared to the RCM12
 442 extreme events. For the CPM2 Top 100 events, which by Maximum Intensity are less intense than RCM12
 443 events, the higher Mean Intensities indicate that the CPM2 events overall are more intense than the RCM12
 444 events, while the RCM12 events seem to have a more peaked intensity distribution (again consistent with these
 445 being associated with grid-points storms in some cases).

446 For the seasonal median SEE the Top 100, Top 1,000 and Top 10,000 events for each season are sampled.
 447 Seasonal median SEE_{max} for Top 100 shows the largest difference between the RCM12 and CPM2 dataset for
 448 autumn and winter events (Fig. 9a,d). By contrast spring and summer events are less different for the Top 100

449 events (Fig. 9b,c). The same pattern is observed for the seasonal SEE_{mean} for Top 100 events (Fig. 9e-h). For
 450 each seasons' Top 100 events, the CPM2 exhibits lower intensity in the SEE_{max} compared to the RCM12, which
 451 corresponds well with the results found in Fig. 8a. Analysing seasonal SEE_{max} and SEE_{mean} for Top 1,000 and
 452 Top 10,000 show the largest difference between datasets for summer events with higher intensities in the CPM2
 453 dataset and larger area in the RCM12 dataset (Fig. 9). Interestingly SEE_{max} winter events in Top 1,000 and Top
 454 10,000 have larger intensities in the RCM12 data than the CPM2 data, as opposed to the other seasons (Fig. 9a).
 455 The absence of the convective parameterisation scheme in the CPM2 is expected to result in a large difference
 456 in summer events between the two models, as it is in this season most convective events develop in the case
 457 area. The low winter intensities and small areas of the CPM2 compared to the RCM12 (mostly for Top 100 and
 458 Top 1,000) could indicate that the difference in rainfall modelling in the two models also plays a large role for
 459 winter events.



460
 461 **Fig. 9** Simplified evolution based on maximum intensity (SEE_{max} , (a)-(d)) and mean intensity (SEE_{mean} , (e)-(h)). (a), (e):
 462 winter events (DJF), (b), (f): spring events (MAM), (c), (g): summer events (JJA) and (d), (h): autumn events (SON). Top
 463 100, Top 1,000 and Top 10,000 within each season is shown with dashed, dotted and solid lines respectively. Data for both
 464 CPM2 (black triangles) and RCM12 (grey circles) are shown.

465 4. Conclusion

466 The difference in the representation of extreme events between an RCM12 and a CPM2 was analysed by
 467 applying a storm tracking algorithm to the two datasets. Extreme events in the Northern European case area
 468 were found to have very different storm tracks, both in terms of location of the tracks, location of the peak
 469 maximum intensity, and movement direction. The largest differences were found for the most severe extreme
 470 events, indicating completely different sets of extreme events between the two models. This corresponds well
 471 with a recent ensemble study of CPMs and RCMs, which found the greatest improvements in the performance
 472 of CPMs for heavy precipitation events (Ban et al. 2021). It is also consistent with earlier studies showing the
 473 improved representation of hourly precipitation extremes in CPMs, due to the improved representation of
 474 convection (Kendon et al. 2014). For the most intense RCM12 events, these were to a large extent captured in
 475 the CPM2 but with lower intensities, whilst the most intense CPM2 events were largely absent in the RCM12.
 476 The most intense events in RCM12 are considered unphysical, and likely due to grid point storms (Chan et al.
 477 2014c). Seasonal differences also illustrate the differences between the models. Here it was found that the

478 RCM12 data have a larger fraction of non-summer events in the extreme event set compared to the CPM2 data.
479 These differences between models were not found when sampling events by maximum area, i.e. events that are
480 spatially large but not necessarily intense. Analysing the coincidence of large and intense events showed a larger
481 fraction of the events sampled as both intense and spatially large in the RCM12 dataset compared to the CPM2
482 dataset. In summary, the extremes of the two models have low correspondence with each other.

483 Analysing time series of area, volume, maximum intensity and mean intensity for the Top 100 most extreme
484 events over the lifetime of the event, showed large differences between the models. Large differences in the area
485 of the extreme events explained the model differences in event volume. The CPM2 produces a larger total
486 volume of rainfall within the case area compared to the RCM12 due to higher mean intensities. In the RCM12,
487 extreme events contribute proportionally more to the total volume than in the CPM2, due to their larger spatial
488 size. These differences are again consistent with the expected different character of heavy rainfall in convection-
489 permitting models (which tends to be more intense, Ban et al. (2021)) compared to convection-parameterised
490 models (where heavy rain events are not heavy enough, but tend to be too persistent and widespread, Kendon et
491 al. (2012)). Crook et al. (2019) found an improved contribution to total rainfall volume from MCSs in
492 convection-permitting simulations, compared to convection-parameterised simulations over West Africa.

493 In this study we have developed a method of simplifying area-intensity diagrams to allow the typical event
494 evolution to be visualised across many events with different durations. This makes the method suitable in a
495 climate context and is valuable in assessing differences in the underlying processes. Using the median
496 Simplified Event Evolution showed large differences between RCM12 and CPM2 extreme events. The
497 differences were again largest for the most intense events (Top 100). The Top 100 RCM12 extreme events had
498 higher maximum intensities and areas than CPM2 extreme events, and these events in the RCM12 dataset are
499 likely to be influenced by grid-point storms. For less extreme indices, i.e., the Top 1,000 and Top 10,000 events,
500 extreme events in the CPM2 data were more intense. In general, on the basis of the results here, we conclude
501 that we should have low confidence in the most (Top 100) extreme precipitation events on hourly timescales in
502 convection parameterised RCMs.

503 Sampling extreme events by season showed the largest differences between models in autumn and winter for
504 Top 100 events. For Top 1,000 and Top 10,000 large differences between models were found for summer
505 events, which was expected due to the differences between the models in how convection is represented, and
506 convection having greatest impact in this season. The large difference in winter extreme events was less
507 expected, with lower intensities for the CPM2 events compared to the RCM12. This indicates that the difference
508 in the representation of convection between models does not only affect events in summer. In addition to the
509 representation of convection, the finer grid spacing of the CPM2 may allow it to better represent mesoscale
510 structures within fronts, thereby impacting frontal events in winter.

511 The analysis performed on coarser resolution data (regridding model data to 25 km resolution before tracking)
512 did not explain differences in event track location and event evolution found between models in the 12km data.
513 We conclude that the difference between the models in how they represent rainfall strongly influences the event
514 characteristics reported here.

515 While no suitable observational dataset was found to analyse the entire region for hourly data, comparing the
516 location of storm tracks and their seasonal distribution against previous observational studies (Morel and Senesi
517 2002) suggests a better performance of the CPM2 compared to the RCM12. This work emphasises the large
518 difference in representation of extreme events between convection-permitting and convection-parameterised
519 models. Using results from a tracking algorithm gives the advantage of analysing the difference in extreme
520 precipitation from an event perspective, which is here explored with a simple visual method, the Simplified
521 Event Evolution. The influence of grid-point storms in the RCM12 dataset shows that analysing and comparing
522 extreme events from the RCM12 dataset should be treated with care. Overall there are indications that the
523 CPM2 is more reliable in representing hourly extremes than the RCM12, based on previous studies comparing
524 with observations. The methods used in this study could additionally be used to compare differences in the
525 representation of extreme events between models in future projections.

526

527 **5. Declarations**

528 **5.1. Funding**

529 Emma D. Thomassen received funding from the Danish State through the Danish Climate Atlas. Elizabeth
530 Kendon gratefully acknowledges funding from the Joint UK BEIS/Defra Hadley Centre Climate Programme
531 (GA01101) and funding from the European Union under Horizon 2020 project European Climate Prediction
532 System (EUCP; Grant agreement: 776613). Steven C. Chan gratefully acknowledges funding from United
533 Kingdom NERC (FUTURE-STORMS; grant: NE/R01079X/1) and European Research Council (INTENSE;
534 grant: ERC-2013-CoG-617329). Peter L. Langen's contributions were funded by the Aarhus University
535 Interdisciplinary Centre for Climate Change (iClimate). Ole B. Christensen's contributions were partly funded
536 by the Danish state through the National Centre for Climate Research (NCKF).

537 **5.2. Conflicts of interest/Competing interests**

538 The authors declare that they have no competing interests.

539 **5.3. Availability of data and material**

540 Model data are available upon request from the UK Met Office, which are used under licence and there are
541 restrictions on their use. The Europe 2.2km data is being analysed as part of the EUCP project, and use of these
542 data must respect the work plans of the EUCP project partners.

543 **5.4. Code availability**

544 The data analysis was carried out using open-source software R and Python.

545 6. References

- 546 Archer DR, Fowler HJ (2015) Characterising flash flood response to intense rainfall and impacts using historical
547 information and gauged data in Britain. *J Flood Risk Manag* 11:S121–S133.
548 <https://doi.org/10.1111/jfr3.12187>
- 549 Ban N, Caillaud C, Coppola E, et al (2021) The first multi-model ensemble of regional climate simulations at
550 kilometer-scale resolution, part I: evaluation of precipitation. *Clim Dyn* 34:35.
551 <https://doi.org/10.1007/s00382-021-05708-w>
- 552 Ban N, Schmidli J, Schär C (2014) Evaluation of the convection-resolving regional climate modeling approach
553 in decade-long simulations. *J Geophys Res Atmos* 119:7889–7907. <https://doi.org/10.1002/2014JD021478>
- 554 Berthou S, Kendon EJ, Chan SC, et al (2018) Pan-European climate at convection-permitting scale: a model
555 intercomparison study. *Clim Dyn* 55:35–59. <https://doi.org/10.1007/s00382-018-4114-6>
- 556 Boutle IA, Abel SJ, Hill PG, Morcrette CJ (2014a) Spatial variability of liquid cloud and rain: observations and
557 microphysical effects. *Q J R Meteorol Soc* 140:583–594. <https://doi.org/10.1002/qj.2140>
- 558 Boutle IA, Eyre JEJ, Lock AP (2014b) Seamless stratocumulus simulation across the turbulent gray zone. *Mon*
559 *Weather Rev* 142:1655–1668. <https://doi.org/10.1175/MWR-D-13-00229.1>
- 560 Brisson E, Brendel C, Herzog S, Ahrens B (2018) Lagrangian evaluation of convective shower characteristics in
561 a convection-permitting model. *Meteorol Zeitschrift* 27:59–66. <https://doi.org/10.1127/METZ/2017/0817>
- 562 Caillaud C, Somot S, Alias A, et al (2021) Modelling Mediterranean heavy precipitation events at climate scale:
563 an object-oriented evaluation of the CNRM-AROME convection-permitting regional climate model. *Clim*
564 *Dyn* 56:1717–1752. <https://doi.org/10.1007/s00382-020-05558-y>
- 565 Caine S, Lane TP, May PT, et al (2013) Statistical assessment of tropical convection-permitting model
566 simulations using a cell-tracking algorithm. *Mon Weather Rev* 141:557–581.
567 <https://doi.org/10.1175/MWR-D-11-00274.1>
- 568 Chan SC, Kendon EJ, Fowler HJ, et al (2014a) Projected increases in summer and winter UK sub-daily
569 precipitation extremes from high-resolution regional climate models. *Environ Res Lett* 9:.
570 <https://doi.org/10.1088/1748-9326/9/8/084019>
- 571 Chan SC, Kendon EJ, Fowler HJ, et al (2014b) The Value of High-Resolution Met Office Regional Climate
572 Models in the Simulation of Multihourly Precipitation Extremes. *J Clim* 27:6155–6174.
573 <https://doi.org/10.1175/JCLI-D-13-00723.1>
- 574 Chan SC, Kendon EJ, Fowler HJ, et al (2014c) The Value of High-Resolution Met Office Regional Climate
575 Models in the Simulation of Multihourly Precipitation Extremes. *J Clim* 27:6155–6174.
576 <https://doi.org/10.1175/JCLI-D-13-00723.1>
- 577 Christensen JH, Christensen OB (2003) Severe summertime flooding in Europe. *Nature* 421:805–806.
578 <https://doi.org/10.1038/421805a>
- 579 Clark P, Roberts N, Lean H, et al (2016) Convection-permitting models: a step-change in rainfall forecasting.
580 *Meteorol Appl* 23:165–181. <https://doi.org/10.1002/met.1538>
- 581 Crook J, Klein C, Folwell S, et al (2019) Assessment of the Representation of West African Storm Lifecycles in
582 Convection-Permitting Simulations. *Earth Sp Sci* 6:818–835. <https://doi.org/10.1029/2018EA000491>
- 583 Dee DP, Uppala SM, Simmons AJ, et al (2011) The ERA-Interim reanalysis: Configuration and performance of
584 the data assimilation system. *Q J R Meteorol Soc* 137:553–597. <https://doi.org/10.1002/qj.828>
- 585 Frei C, Schöll R, Fukutome S, et al (2006) Future change of precipitation extremes in Europe: Intercomparison
586 of scenarios from regional climate models. *J Geophys Res Atmos* 111:.
587 <https://doi.org/10.1029/2005JD005965>
- 588 Gregory D, Rowntree PR (1990) A mass flux convection scheme with representation of cloud ensemble
589 characteristics and stability-dependent closure. *Mon Weather Rev* 118:1483–1506.
590 [https://doi.org/10.1175/1520-0493\(1990\)118<1483:AMFCSW>2.0.CO;2](https://doi.org/10.1175/1520-0493(1990)118<1483:AMFCSW>2.0.CO;2)
- 591 Haralick RM, Shapiro L (1992) *Computer and Robot Vision, Vol I, 1st edn.* Addison-Wesley Longman

- 593 IPCC (2012) *Managing the Risks of Extreme Events and Disasters to Advance Climate Change Adaptation*. A
594 Special Report of Working Groups I and II of the Intergovernmental Panel on Climate Change.
595 Cambridge, UK, and New York, NY, USA
- 596 Keat WJ, Stein THM, Phaduli E, et al (2019) Convective initiation and storm life cycles in convection-
597 permitting simulations of the Met Office Unified Model over South Africa. *Q J R Meteorol Soc*
598 145:1323–1336. <https://doi.org/10.1002/qj.3487>
- 599 Kendon EJ, Ban N, Roberts NM, et al (2017) Do Convection-Permitting Regional Climate Models Improve
600 Projections of Future Precipitation Change? *Bull Am Meteorol Soc* 98:79–93.
601 <https://doi.org/10.1175/BAMS-D-15-0004.1>
- 602 Kendon EJ, Prein AF, Senior CA, Stirling A (2021) Challenges and outlook for convection-permitting climate
603 modelling. *Philos Trans R Soc A Math Phys Eng Sci* 379:. <https://doi.org/10.1098/rsta.2019.0547>
- 604 Kendon EJ, Roberts NM, Fowler HJ, et al (2014) Heavier summer downpours with climate change revealed by
605 weather forecast resolution model. *Nat Clim Chang* 4:570–576. <https://doi.org/10.1038/nclimate2258>
- 606 Kendon EJ, Roberts NM, Senior CA, Roberts MJ (2012) Realism of Rainfall in a Very High-Resolution
607 Regional Climate Model. *J Clim* 25:5791–5806. <https://doi.org/10.1175/JCLI-D-11-00562.1>
- 608 Li L, Li Y, Li Z (2020) Object-based tracking of precipitation systems in western Canada: the importance of
609 temporal resolution of source data. *Clim Dyn* 55:2421–2437. <https://doi.org/10.1007/s00382-020-05388-y>
- 610 Lucas-Picher P, Wulff-Nielsen M, Christensen JH, et al (2012) Very high resolution regional climate model
611 simulations over Greenland: Identifying added value. *J Geophys Res Atmos* 117:.
612 <https://doi.org/10.1029/2011JD016267>
- 613 Molinari J, Dudek M (1992) Parameterization of Convective Precipitation in Mesoscale Numerical Models: A
614 Critical Review. *Mon Weather Rev* 120:326–344. [https://doi.org/10.1175/1520-0493\(1992\)120<0326:POCPIM>2.0.CO;2](https://doi.org/10.1175/1520-0493(1992)120<0326:POCPIM>2.0.CO;2)
- 616 Morel C, Senesi S (2002) A climatology of mesoscale convective systems over Europe using satellite infrared
617 imagery. II: Characteristics of European mesoscale convective systems. *Q J R Meteorol Soc* 128:1973–
618 1995. <https://doi.org/10.1256/003590002320603494>
- 619 Prein AF, Gobiet A, Suklitsch M, et al (2013) Added value of convection permitting seasonal simulations. *Clim*
620 *Dyn* 41:2655–2677. <https://doi.org/10.1007/s00382-013-1744-6>
- 621 Prein AF, Langhans W, Fosser G, et al (2015) A review on regional convection-permitting climate modeling:
622 Demonstrations, prospects, and challenges. *Rev. Geophys.* 53:323–361
- 623 Prein AF, Liu C, Ikeda K, et al (2017a) Increased rainfall volume from future convective storms in the US. *Nat*
624 *Clim Chang* 7:880–884. <https://doi.org/10.1038/s41558-017-0007-7>
- 625 Prein AF, Liu C, Ikeda K, et al (2017b) Simulating North American mesoscale convective systems with a
626 convection-permitting climate model. *Clim Dyn* 1–16. <https://doi.org/10.1007/s00382-017-3993-2>
- 627 Prein AF, Rasmussen RM, Ikeda K, et al (2017c) The future intensification of hourly precipitation extremes.
628 *Nat Clim Chang* 7:48–52. <https://doi.org/10.1038/nclimate3168>
- 629 Purr C, Brisson E, Ahrens B (2019) Convective shower characteristics simulated with the convection-permitting
630 climate model COSMO-CLM. *Atmosphere (Basel)* 10:810. <https://doi.org/10.3390/ATMOS10120810>
- 631 Rinehart RE, Garvey ET (1978) Three-dimensional storm motion detection by conventional weather radar.
632 *Nature* 273:287–289. <https://doi.org/10.1038/273287a0>
- 633 Rosenzweig B, Ruddell BL, McPhillips L, et al (2019) Developing knowledge systems for urban resilience to
634 cloudburst rain events. *Environ Sci Policy* 99:150–159. <https://doi.org/10.1016/j.envsci.2019.05.020>
- 635 Rummukainen M (2010) State-of-the-art with regional climate models. *Wiley Interdiscip. Rev. Clim. Chang.*
636 1:82–96
- 637 Semadeni-Davies A, Hernebring C, Svensson G, Gustafsson LG (2008) The impacts of climate change and

638 urbanisation on drainage in Helsingborg, Sweden: Combined sewer system. *J Hydrol* 350:100–113.
639 <https://doi.org/10.1016/j.jhydrol.2007.05.028>

640 Smith RNB (1990) A scheme for predicting layer clouds and their water content in a general circulation model.
641 *Q J R Meteorol Soc* 116:435–460. <https://doi.org/10.1002/qj.49711649210>

642 Stein THM, Hogan RJ, Hanley KE, et al (2014) The Three-Dimensional Morphology of Simulated and
643 Observed Convective Storms over Southern England. *Mon Weather Rev* 142:3264–3283.
644 <https://doi.org/10.1175/MWR-D-13-00372.1>

645 Sunyer MA, Luchner J, Onof C, et al (2017) Assessing the importance of spatio-temporal RCM resolution when
646 estimating sub-daily extreme precipitation under current and future climate conditions. *Int J Climatol*
647 37:688–705. <https://doi.org/10.1002/joc.4733>

648 Thorndahl S, Einfalt T, Willems P, et al (2017) Weather radar rainfall data in urban hydrology. *Hydrol Earth*
649 *Syst Sci* 21:1359–1380. <https://doi.org/10.5194/hess-21-1359-2017>

650 Trenberth KE, Dai A, Rasmussen RM, Parsons DB (2003) The changing character of precipitation. *Bull Am*
651 *Meteorol Soc* 84:1205–1217. <https://doi.org/10.1175/BAMS-84-9-1205>

652 Urich C, Rauch W (2014) Exploring critical pathways for urban water management to identify robust strategies
653 under deep uncertainties. *Water Res* 66:374–389. <https://doi.org/10.1016/j.watres.2014.08.020>

654 Williams KD, Copsey D, Blockley EW, et al (2018) The Met Office Global Coupled Model 3.0 and 3.1 (GC3.0
655 and GC3.1) Configurations. *J Adv Model Earth Syst* 10:357–380. <https://doi.org/10.1002/2017MS001115>

656 Wilson DR, Bushell AC, Kerr-Munslow AM, et al (2008) PC2: A prognostic cloud fraction and condensation
657 scheme. I: Scheme description. *Q J R Meteorol Soc* 134:2093–2107. <https://doi.org/10.1002/qj.333>

658

659